Biosensors and Bioelectronics 183 (2021) 113208

Contents lists available at ScienceDirect

Biosensors and Bioelectronics

journal homepage: http://www.elsevier.com/locate/bios

A graphene oxide-based fluorescent nanosensor to identify antiviral agents via a drug repurposing screen

Hojeong Shin [a], Se-Jin Park [a], Jungho Kim [a], Ji-Seon Lee [a], Dal-Hee Min [a,b,c,*]

[a] Department of Chemistry, Seoul National University, Seoul, 08826, Republic of Korea
[b] Department of Biological Sciences, Seoul National University, Seoul, 08826, Republic of Korea
[c] Institute of Biotherapeutics Convergence Technology, Lemonex Inc., Seoul, 08826, Republic of Korea

ARTICLE INFO

Keywords:
Biosensor
Dengue virus
Drug repurposing
Graphene oxide
High-throughput screening

ABSTRACT

Currently, there are no approved therapeutics for Dengue virus (DENV) infection, even though it can cause fatal complications. Understanding DENV infection and its propagation process in host cells is necessary to develop specific antiviral therapeutics. Here, we developed a graphene oxide-based fluorescent system (**G**raphene **O**xide-based **Vi**ral **R**NA **A**nalysis system, **GOViRA**) that enables sensitive and quantitative real-time monitoring of the intracellular viral RNA level in living cells. The GOViRA system consists of a fluorescent dye-labeled peptide nucleic acid (PNA) with a complementary sequence to the DENV genome and a dextran-coated reduced graphene oxide nanocolloid (DRGON). When the dye labeled PNA is adsorbed onto DRGON, the fluorescence of the dye is effectively quenched. The quenched fluorescence signal is recovered when the dye labeled PNA forms interaction with intracellular viral RNA in DENV infected host cells. We demonstrated the successful use of the GOViRA platform for high-throughput screening to discover novel antiviral compounds. Through a cell-based high-throughput screening of FDA-approved small-molecule drugs, we identified ulipristal, a selective progesterone receptor modulator (SPRM), as a potent inhibitor against DENV infection. The anti-DENV activity of ulipristal was confirmed both *in vitro* and *in vivo*. Moreover, we suggest that the mode of action of ulipristal is mediated by inhibiting viral entry into the host cells.

1. Introduction

Dengue virus (DENV) is a member of the *Flavivirus* genus which includes the Zika virus (ZIKV), Japanese encephalitis virus (JEV), yellow fever virus (YFV), West Nile virus (WNV), and tick-borne virus (TBEV) (Kuno et al., 1998). DENV, the most widespread arthropod-borne virus, is a serious human pathogen and one of the major concerns in the global public health because it causes over 300 million infection cases annually. DENV infection causes clinical symptoms that range from subclinical mild dengue fever to severe dengue such as dengue hemorrhage fever (DHF) and dengue shock syndrome (DSS) accompanied by severe bleeding, organ impairment, and plasma leakage which can lead to death (Martina et al., 2009; Wilder-Smith et al., 2019). Unfortunately, there is no approved drug or specific therapy for DENV infection up to now. The discovery of novel medications against DENV is required to resolve DENV-induced public health issues.

The conventional methods of developing antiviral agents require massive resources including time, money, and labor. Due to these limitations, tropical diseases are often neglected and disregarded by the pharmaceutical industry. Drug repurposing (or 'drug repositioning'), finding effective agents from approved drugs, has appeared as an efficient way of identifying potential medications (Pushpakom et al., 2019). To identify the efficacy of antiviral drug candidates on virus-infected cells, a variety of *in vitro* assay systems have received much attention: viral infectivity assays (focus-forming assay (FFA), plaque assay, and yield reduction assay) (Herzog et al., 2008; Ye et al., 2019), methods measuring the viral genome and proteins (quantitative reverse transcription-PCR (qRT-PCR) and immunostaining) (Barrows et al., 2016; Garcia et al., 2001), and methods using a gene-modified virus (reporter virus particles (RVP) and virus-like particles (VLP) (Qing et al., 2010; Zou et al., 2011). However, these *in vitro* assay systems have shown several limitations, including low reproducibility, high costs, labor-intensive process, and/or viral genetic modifications. Because of these limitations, they are not suitable for repurposing drugs through high-throughput screening. Therefore, new assays that enable a sensitive cell-level analysis of viral infection using native virus with an

* Corresponding author. Department of Chemistry, Seoul National University, Seoul, 08826, Republic of Korea.
E-mail address: dalheemin@snu.ac.kr (D.-H. Min).

https://doi.org/10.1016/j.bios.2021.113208
Received 14 December 2020; Received in revised form 23 March 2021; Accepted 28 March 2021
Available online 1 April 2021

unmodified genome are in demand.

DENV has a single-stranded RNA genome that encodes three structural (C, prM/M, and E) proteins and seven nonstructural (NS1, NS2A, NS2B, NS3, NS4A, NS4B, and NS5) proteins (Boldescu et al., 2017; Wilder-Smith et al., 2019). When mammalian cells are inoculated with DENV, membrane fusion occurs due to the acidic environment of the endosome, and genomic RNA is released into the cytoplasm sequentially. After the release of the RNA, a single open reading frame (ORF) is translated into viral polyproteins, and a replication complex is assembled on the cytoplasmic side of the endoplasmic reticulum (ER) membrane. Then, NS5 protein, the RNA-dependent RNA polymerase (RdRp), produces numerous copies of viral genomic RNA in the cytoplasm of the host cell, and the produced viral RNA is translated into the viral polypeptides. The immature DENV particles are transported through the trans-Golgi network (TGN) where they are converted into infectious form and they are released from the host cell. The number of viral RNA copies in the cytoplasm directly reflects any change that occurred in the viral infection or proliferation process. Therefore, monitoring the change in the intracellular viral RNA level is an efficient method to analyze DENV infection.

Herein, we designed a real-time DENV infection analysis system (**G**raphene **O**xide-based **Vi**ral **R**NA **A**nalysis system, abbreviated as **GOViRA**) using a fluorescent dye-labeled peptide nucleic acid (PNA) and a dextran-coated reduced graphene oxide nanocolloid (DRGON) that can directly monitor and quantify intracellular viral RNA in living cells (Fig. 1). Graphene oxide (GO)-based nanomaterials have been actively used in developing a wide range of sensors because of their physicochemical properties (Goldoni et al., 2021; Hwa et al., 2020; Sharma and Hwa 2020). In this strategy, DRGON acts as both a delivery carrier and a quencher of the dye-labeled PNA probe (Loh et al., 2010; Ryoo et al., 2013). When the dye-labeled PNA is adsorbed onto DRGON by the π–π interaction and hydrogen bonding (Park et al., 2013; Xu et al., 2017), the fluorescence of the dye is effectively quenched through fluorescence resonance energy transfer (FRET). The introduction of the target viral genome induces the detachment of the PNA probe that has the complementary sequence to the viral genome and leads to the recovery of the fluorescence signal because of the high affinity and specificity of PNA to viral RNA. Therefore, when the mammalian cells are infected with DENV, several copies of viral RNA, the target of the GOViRA system, are replicated in the cytosol, and the dye labeled PNA is hybridized with the viral RNA resulting in the release of the PNA probe from DRGON. The observation of DENV infection with the GOViRA platform does not require terminal processing of the cells (e.g., fixation and lysis). These advantages offer real-time visualization and the analysis of DENV infection in live cells.

Moreover, we demonstrated that the GOViRA platform is suitable for antiviral discovery screening. The GOViRA system can discover drug candidates associated with both viral and host pathways related to the viral life cycle. Since the GOViRA platform does not require viral genome engineering, it offers great strength in targeting the complete life cycle of the native virus. To address the urgent need for anti-DENV agents, we conducted a cell-based screening of the Food and Drug Administration (FDA)-approved drugs. Through the screening, we successfully identified a novel class of a small-molecule anti-DENV compound, ulipristal, which is previously known as a selective progesterone receptor modulator (SPRM). Used for emergency contraception (Richardson and Maltz 2012) or treatment of uterine fibroids (Donnez et al., 2015), ulipristal has never been reported to have an antiviral activity against any kind of virus. After a series of evaluations, we confirmed that ulipristal not only has an anti-DENV activity both *in vitro* and *in vivo* but also inhibits DENV entry into the host cell.

2. Materials and methods

2.1. Reagents and apparatus

Graphite nanofiber was purchased from Carbon Nano-materials Technology. Potassium persulfate ($K_2S_2O_8$), phosphorus pentoxide (P_2O_5), and hydrogen peroxide (H_2O_2, 30%) were purchased from Junsei. Potassium permanganate ($KMnO_4$) and ammonium hydroxide (NH_4OH) were purchased from Sigma-Aldrich. Sulfuric acid (H_2SO_4) and hydrochloric acid (HCl) were purchased from Samchun chemical. Dextran was purchased from Fluka. Ribavirin and ulipristal were purchased from Sigma-Aldrich.

2.2. Synthesis and characterization of DRGON

DRGON was synthesized according to previously published method (Lee et al., 2016). The height profiles were obtained by an atomic force microscope (AFM) NX-10 (Park Systems). FT-IR measurement was

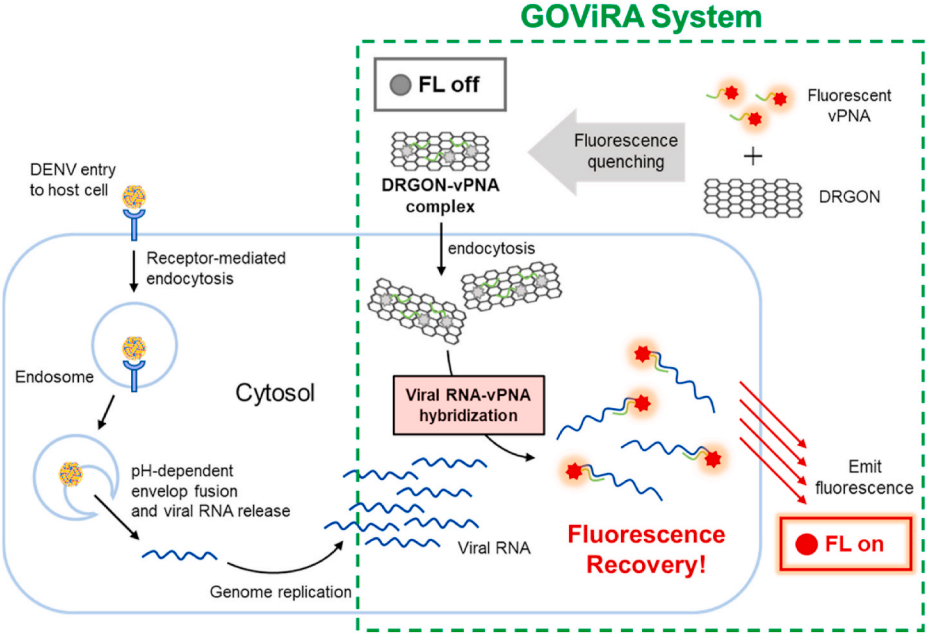

Fig. 1. The strategy for real-time DENV genome monitoring GOViRA platform.

conducted by a FT-IR spectrometer NICoLET iS10 (Thermo Scientific). The UV–Vis absorbance spectra and PL spectra were obtained by the S-3100 (Scinco) and the ACTON SpectraPro 2150i spectrometer (Princeton Instruments), respectively. The X-ray diffraction (XRD) patterns were obtained using a D8 Advanced (Bruker) system with Cu-Kα radiation (1.54 Å). Raman spectra were obtained by LabRAM HR UV/vis/NIR (Horiba Jobin Yvon) with an Ar ion CW laser (514.5 nm) as an excitation source focused through a BXFM confocal microscope with an objective lens (50X, numerical aperture = 0.50). The average particle size and zeta potential were measured with the Zetasizer Nano S DLS analyzer (Malvern Panalytical). The TEM images were acquired using a H-7600 (Hitachi) at 100 kV. Energy-dispersive X-ray spectroscopy (EDS) analysis was performed by JEM-F200 (JEOL Ltd).

2.3. Quenching and recovery of the fluorescence signal of PNA probe using DRGON

First, 20 pmol Cy5-labeled PNA probe (Panagene) was mixed with an increasing amount of DRGON in 1x PBS and incubated for 10 min at RT. The fluorescence intensity of Cy5 (Ex/Em = 650/670 nm) was measured after the formation of the PNA-DRGON complex. To evaluate the specificity of the PNA-DRGON complex, single-stranded RNA (Bioneer) was added to the complex. The fluorescence signal was monitored by SynergyMx (Biotek).

2.4. Cell culture and viruses

Vero E6 was kindly provided by Professor K. Ahn from the Department of Biological Sciences, Seoul National University. The Vero E6 and Huh7 (Korean Cell Line Bank, 60104) cells were maintained in DMEM supplemented with 10% fetal bovine serum (FBS) and P/S. A549 (ATCC, CCL-185) cells were maintained in RPMI supplemented with 10% FBS and P/S.

DENV serotype 1 (DenKor-07) was purchased from the National Culture Collection for Pathogens, Korea. DENV serotype 2, 3, 4, and JEV (KBPV-VR-29, KBPV-VR-30, KVPV-VR-31, and KBPV-VR-27) were purchased from the Korea Bank for Pathogenic Viruses. ZIKV (Zika/Brazil/16321) was purchased from the Virus Research and Testing Center, Korea. DENV, ZIKV, and JEV were amplified in the Vero E6 cells with DMEM supplemented with 2% FBS and P/S. The cells were inoculated with a MOI of 0.05. The virus-containing media was cleared by centrifugation at 2000 g for 10 min, and aliquots were stored at −80 °C.

2.5. Focus-forming assays (FFA)

The virus was titrated by FFA in Vero E6 cells. Ten-fold serial diluted virus in DMEM supplemented with 2% FBS and P/S was added onto confluent Vero E6 cell monolayers attached to 96-well, black wall, optical bottom plates (Corning) and incubated for 1 h. After the incubation, the wells were overlaid with 100 μL of DMEM with 10% FBS, P/S, and methylcellulose and incubated for 2 days. Following the incubation, cell monolayers were fixed with 4% paraformaldehyde and then treated with blocking solution for 1 h. Samples were then treated with the anti-Dengue virus E protein antibody (GeneTex, GTX127277), followed by FITC-labeled goat anti-mouse IgG secondary antibody (Sigma-Aldrich, F0257).

2.6. Live-cell imaging

Vero E6 cells were seeded onto 96-well, black wall, optical bottom plates at a density of 1.5 x 10^4 cells per well and incubated with DMEM supplemented with 10% FBS and P/S. After overnight incubation, the cells were briefly washed with 1x PBS and infected with DENV. Next, 20 pmol vPNA or β-actin PNA probe was mixed with 1.2 μg DRGON solution for 10 min at RT. The Vero E6 cells were treated with the PNA-DRGON complexes for 5 h. The plates were incubated for up to 72 h, and cell nuclei were counterstained with Hoechst 33342. Fluorescent images were obtained by the IN Cell Analyzer 2000 (GE Healthcare) and DeltaVision Elite (GE Healthcare) imaging system. The quantification of data was processed with the IN Cell Developer software (https://cyvitalifesciences.com).

2.7. Cell viability test

The CCK-8 assay was performed according to the manufacturer's instructions. Vero E6, Huh7, and A549 cells were seeded in 96-well culture plates with 100 μL of complete media. After 24 h of incubation, the cells were treated with nanomaterials or drug in serially diluted concentrations for 48 h. The cells were rinsed with 1x PBS twice, and CCK-8 reagent was treated at a concentration of 10% (v/v) and incubated for 1 h. The optical density at 450 nm was measured by SynergyMx (Biotek) in the absorbance mode.

2.8. qRT-PCR analysis

Total RNA was extracted using Trizol (Invitrogen). The cDNA samples were prepared by reverse transcription using SuperScript II Reverse Transcriptase (Invitrogen). The synthesized cDNA samples were subjected to qRT-PCR with primers specific for each gene by using the PowerUp SYBR Green Master Mix (Applied Biosystems) and CFX Connect (Bio-Rad). Primer sequences were confirmed shown in Table S2.

2.9. Drug library screening

For the drug library screening experiments, 1.5 x 10^4 Vero E6 cells in a total volume of 100 μL per well were seeded onto 96-well, black wall, optical bottom plates using DMEM media supplemented with 10% FBS and P/S and incubated overnight. Next, the cells were pretreated with 50 μL of experimental compounds or vehicle in DMEM supplemented with 2% FBS and P/S and incubated 1 h at 37 °C. Next, 50 μL of DENV (a final MOI of 0.5) were added to each well, resulting in a 10 μM final concentration for each compound and cells were incubated for 48 h. Infection was stopped by rinsing each well with 1x PBS, and the infected cells were treated with the PNA-DRGON complexes for 5 h at 37 °C and then briefly washed with 1x PBS. Fluorescent images were obtained by the IN Cell Analyzer 2000, and quantification of the data was processed using the IN Cell Developer software.

2.10. Animal experiments

AG129 mice (8–10 weeks old, female) were purchased from Marshall BioResources and housed under pathogen-free conditions. Animal research was approved by the Institutional Animal Care and Use Committee of Seoul National University and was performed according to the guidelines of the recommendations from the Association for Assessment and Accreditation of Laboratory Animal Care.

2.11. Murine DENV infection model

We described the murine DENV infection model previously (Park et al., 2020). AG129 mice were exposed with a target dose of 10^7 FFU of the DENV by intraperitoneal injection. One hour after the challenge, the animals were treated with ulipristal. The compound was dissolved in sesame oil at a 10x concentration and further diluted in 1x PBS. Ulipristal was administered to the animals by intraperitoneal injection. Animals in the vehicle control groups were administered a solution with no drug. The animals were monitored for weight, morbidity (ruffled fur, hunched posture, etc.), and survival daily for a total of 14 days after infection. Mice with a weight <80% of their initial body weight were humanely euthanized.

At 3 days p.i., mice were sacrificed from each group. Blood and organ samples were collected. Blood was clarified by centrifugation, and

viremia was determined by qRT-PCR. Organs were homogenized, and total RNA was extracted using Trizol. The relative DENV RNA level from each organ was determined by qRT-PCR. Primer sequences were confirmed shown in Table S2.

2.12. Hematoxylin and eosin (H&E) staining

Organ samples were fixed with 4% paraformaldehyde and embedded in paraffin. Paraffin sections were stained with H&E at the pathology core facility in the Center for Medical Innovation, Seoul National University Hospital, Korea.

2.13. Time-of-addition assay

A549 cells were seeded onto 24-well plates. After incubation overnight, cells were treated with ulipristal at the various time points and inoculated with DENV. At 48 h p.i., the cells were washed with 1x PBS and processed for qRT-PCR.

2.14. Statistics

Statistical analysis was conducted using the GraphPad Prism software as described in the indicated figure legends. Statistical significance was assigned when the value of P was <0.05. Error bars indicate the SEM and the number of n indicated in the figure legends.

3. Results

3.1. Characterization of DRGON

We synthesized DRGON by reducing GON with dextran, a biocompatible polysaccharide polymer. AFM analysis with the corresponding height profile shows the thickness of DRGON to be ~6.20 nm which is thicker than that of GON (Fig. S1A). The increase in the height of DRGON is attributed to the dextran coating acquired during the reduction process on the surface of GON.

The FT-IR spectrum of DRGON showed a decreased intensity of the C═O bond stretching peak at 1720 cm^{-1} compared to the spectrum of GON (Fig. S1B). The decrease in the number of carbonyl groups indicates the successful synthesis of DRGON by the reduction process.

The UV–Vis spectra of GON showed an absorption peak at around 230 nm that is due to the $\pi \rightarrow \pi^*$ transitions of the aromatic C═C bonds and a shoulder at around 305 nm assigned to the $n \rightarrow \pi^*$ transitions of the C═O bonds (Fig. S1C). The UV–visible absorption spectra of DRGON showed a red shift from 230 nm to 245 nm implying a complete reduction and restoration of the C═C bonds. The $n \rightarrow \pi^*$ transition absorption peak was diminished in the absorption spectra of DRGON because the C═O bonds were significantly reduced during the reduction process. The UV–Vis absorption spectra were in a good agreement with the FT-IR results.

This observation was further supported by the PL spectra. The PL spectra of GON and DRGON were obtained using an excitation wavelength of 300 nm (Fig. S1D). The strong emission peak at 430 nm is ascribed to the $\pi^* \rightarrow \pi$ transition that is associated with the aromatic C═C bonds. The peak on the right was attributed to the disorder-induced defect states within the π–π^* gap (Chien et al., 2012). The intensity of the peak induced by defect states significantly decreased in the PL spectrum of DRGON implying a significant increase in the formation of sp^2 domains during the reduction process.

The crystal structures of GON and DRGON were characterized by XRD analysis (Fig. S1E). GON exhibited a graphitic peak at $2\theta = 10.8$ with a d-spacing value of 8.2 Å. Although this peak did not appear in the XRD pattern of DRGON, a new peak was observed at $2\theta = 18.5$ with a d-spacing value of 4.8 Å. The significant reduction in the interlayer distance of DRGON compared to that of GON was due to the removal of the oxygen groups through the reduction process.

The Raman spectra showed D and G bands that are typically found in carbon materials (Fig. S1F). The integrated intensity ratio of the D and G bands (I_D/I_G) was increased from 0.82 to 0.86. The average hydrodynamic diameters of GON and DRGON measured by DLS was 34.0 ± 0.5 nm and 48.2 ± 0.8 nm, respectively (Fig. S1G). The lateral dimension of DRGON from the TEM images was smaller than 100 nm (Fig. S1H) and we found a good correlation between the hydrodynamic diameters measured by the DLS and the particle dimension as measured by TEM. The elemental analysis of DRGON was investigated using EDS (Fig. S1I) and the zeta potential of DRGON was −38.0 ± 0.3 mV. Overall, analytical data indicate the successful synthesis of DRGON.

Graphene-related nanomaterials enter cells by endocytosis, and the dispersibility of the particles strongly modulates their cellular uptake (Zhang et al., 2016). The instability of graphene oxide-based nanomaterials in physiological solutions limits their application in biological areas. To investigate the stability of GON, DRGON and PNA-DRGON complex, we dispersed nanoparticles in 1x PBS solution and complete media (Fig. S2A). DRGON and PNA-DRGON complex maintained its suspension both in 1x PBS solution and complete media for 24 h without showing visible aggregation. On the other hand, GON showed particle aggregation and precipitation in both solutions after 1 h. Moreover, no obvious toxicity was measured with DRGON (Fig. S2B). Even at a high concentration of 400 μg/mL, the cell viability remained 85% which is significantly higher than that with GON. These results show that the dextran coating effectively improved the colloidal stability in physiological solutions and reduced its cytotoxicity. Furthermore, these results demonstrate that DRGON is suitable for biological applications.

3.2. Design for the GOViRA, a fluorescence-based DENV detection assay

We then prepared a fluorogenic PNA probe with high selectivity to the DENV genome. Conserved in all four serotypes of DENV but not in other flaviviruses, a region in the 3' untranslated region (UTR) of the viral genome was chosen as the targeting domain of the PNA probe. The PNA probe composition was designed with practical considerations such as probe length, purine content, and intramolecular binding to improve the solubility of the PNA and to reduce the self-aggregation problem (Stender et al., 2002). The PNA probe that was complementary to the selected region of the viral genome was named as vPNA and conjugated with Cy5 (Table S1).

For the development of the GOViRA (Fig. 1), fluorescence quenching and recovery tests were performed using the prepared DRGON and vPNA probe (Fig. S3A). The fluorescence intensity was quenched down to 1% compared to the initial value when 1.2 μg of DRGON were added to 20 pmol of Cy5-labeled vPNA and it maintained its fluorescence intensity for 24 h in the presence of serum (Fig. S3B, C and E). The recovery of the fluorescence was measured using a chemically synthesized single-stranded RNA with the target sequence. The quenched fluorescence of vPNA was recovered when the target RNA was added. To examine the selectivity of the GOViRA system, Cy5-labeled scPNA was prepared with a randomly scrambled, mismatching sequence (Table S1). No fluorescence signal was observed from the scPNA-DRGON complex in the presence of the target RNA. Additionally, when a scrambled sequence of RNA was mixed with the vPNA-DRGON complex, there was no notable observation of fluorescence recovery as well (Figs. S3D and F). These results indicate that the GOViRA system is highly stable and works only in a sequence-specific manner.

3.3. Validation of the GOViRA system in living cells

To investigate the ability of the GOViRA system to visualize DENV infection in live cells, we inoculated Vero E6 cells with DENV serotype 2 for 48 h and then treated them with PNA-DRGON complexes consisting of vPNA or scPNA for the next 5 h. For relative quantification, a PNA probe complementary to β-actin was conjugated with Cy3 to be used as an internal control (Table S1). As the intracellular viral genome was

replicated after the inoculation, DENV-infected Vero E6 cells displayed a distinct fluorescence signal in the cytoplasm after the addition of the vPNA-DRGON complex, whereas that of the non-infected cells showed no fluorescence signal. In contrast, the treatment of the DENV-infected cells with the scPNA-DRGON complex did not lead to any signs of a fluorescence response (Fig. 2A and B), indicating a high target specificity for the GOViRA system in living cells. When we investigated the z-sectioned image in the same plane, the Cy5 signals from the vPNA probe (labeled in red) were mostly observed in the cytoplasmic area (Fig. 2D). Additionally, to verify the reliability of the GOViRA system, the number of viral RNA copies in the cytoplasm was quantified by qRT-PCR under the same experimental conditions. A high amount of viral genome was detected only in the DENV-infected cells (Fig. 2C), which was highly correlative to the results analyzed from the fluorescence signal. Furthermore, the quantified fluorescence signal corresponding to β-actin remained constant indicating that the β-actin is a suitable internal control (Fig. S4).

DENV exists as multiple serotypes (Martina et al., 2009), which exhibit partially conserved sequences. When the sequence of vPNA was designed, the conserved region in all four serotypes was set as a target. To verify the capability of monitoring DENV infection for all four serotypes, the inoculation of DENV serotype 1, 2, 3, or 4 was followed by vPNA-DRGON treatment. Regardless of the serotype, the DENV-infected groups showed a notable fluorescence signal in response to the vPNA-DRGON treatment, whereas those infected with other flaviviruses did not (Fig. S5). These results indicate that the GOViRA system possesses a great specificity against DENV regardless of the serotype, suggesting that this system could also be used to distinguish the infection of DENV from other flaviviruses.

To determine the capacity of the GOViRA system measuring the dynamic changes in intracellular viral RNA expression levels and monitoring the progress of the viral infection (Hu and Bentley 2000; Mukherjee et al., 2016), we monitored the changes in the fluorescence intensity over time. Vero E6 cells inoculated with DENV were treated with the PNA-DRGON complex at a series of time intervals from 12 to 72 h post-infection (p.i.) (Fig. S6A). As shown in Fig. S6B, the fluorescence signal from the cells showed a time-dependent increase, with a high linear correlation ($R^2 = 0.9997$) to the result from the qRT-PCR analysis (Fig. S6C). Next, Vero E6 cells were inoculated with DENV at various multiplicities of infection (MOI) from 0.25 to 2, and the cells were monitored by live-cell microscopy. The quantified fluorescence signal increased in an MOI-dependent manner (Fig. 3B). Such data suggest that the GOViRA platform facilitates not only real-time visualization of DENV-infection but also quantitative analysis of intracellular viral RNA in living cells.

3.4. High-throughput screening of approved drugs to identify compounds with anti-DENV activity

Because the GOViRA platform with living cells was successfully demonstrated, we then tried to verify whether the GOViRA platform is suitable for high-throughput screening. To determine its systemic reliability as a high-throughput screening assay, we used Z′-factor as a statistical parameter (Zhang et al., 1999). The Z′-factor of the GOViRA platform was calculated to be 0.87 from 20 negative and 20 positive controls (Fig. 3C), which can be suggested as evidence of an excellent assay for high-throughput screening. To further verify whether the GOViRA system is capable of the quantitative analysis of antiviral activity, we utilized the system to investigate the cellular effect caused by a model representative antiviral compound, Ribavirin (Crance et al., 2003). The introduction of the ribavirin induced a serial decrease in the fluorescence signal dose-dependently (Fig. 3D), indicating that the GOViRA system is suitable as a fluorescence-based quantitative antiviral assay.

Using the GOViRA system, we conducted a cell-based screening on a library of ~550 FDA-approved drugs to find therapeutic candidates with

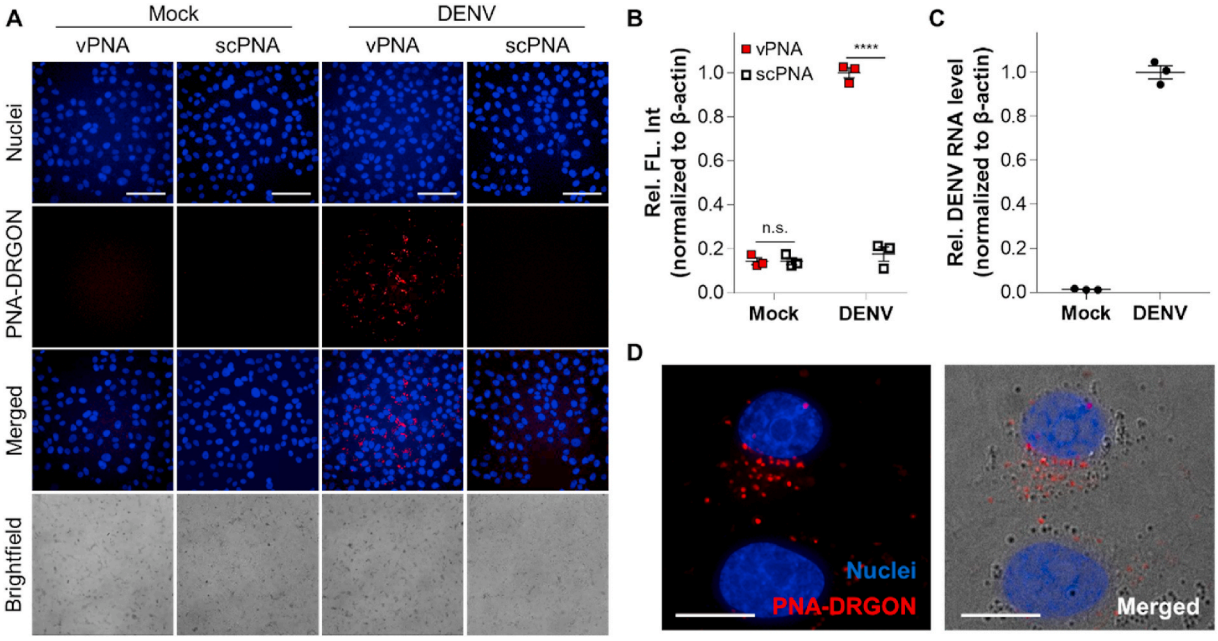

Fig. 2. Qualitative and quantitative detection of the intracellular DENV genome through the GOViRA system in non-infected and DENV-infected Vero E6 cells. (A) Fluorescence images of non-infected and DENV-infected Vero E6 cells were taken after 5 h of PNA-DRGON complex treatment. PNA-DRGON complex was introduced at 48 h p.i. that including Cy5 labeled vPNA or scPNA. Scale bar: 25 μm. (Red, Cy5 signals from PNA probe; Blue, Hoechst signals from nuclei) (B) Quantitative analysis of Cy5 signals from PNA-DRGON complexes treated in non-infected and DENV-infected Vero E6 cells. The relative intensity of each signal was normalized to the β-actin signal as an internal control. Values represent mean ± SEM (n = 3). Statistical significance was determined by Student's *t*-test (n.s.: not significant, $^{****}P \leq 0.0001$). (C) qRT-PCR analysis for the expression of the DENV genome in Vero E6 cells. Values represent mean ± SEM (n = 3). (D) Fluorescence images of DENV-infected Vero E6 cells were taken after 5 h of vPNA-DRGON complex treatment with DeltaVision microscope. Scale bar: 15 μm. (Red, Cy5 signals from PNA probe; Blue, Hoechst signals from nuclei).

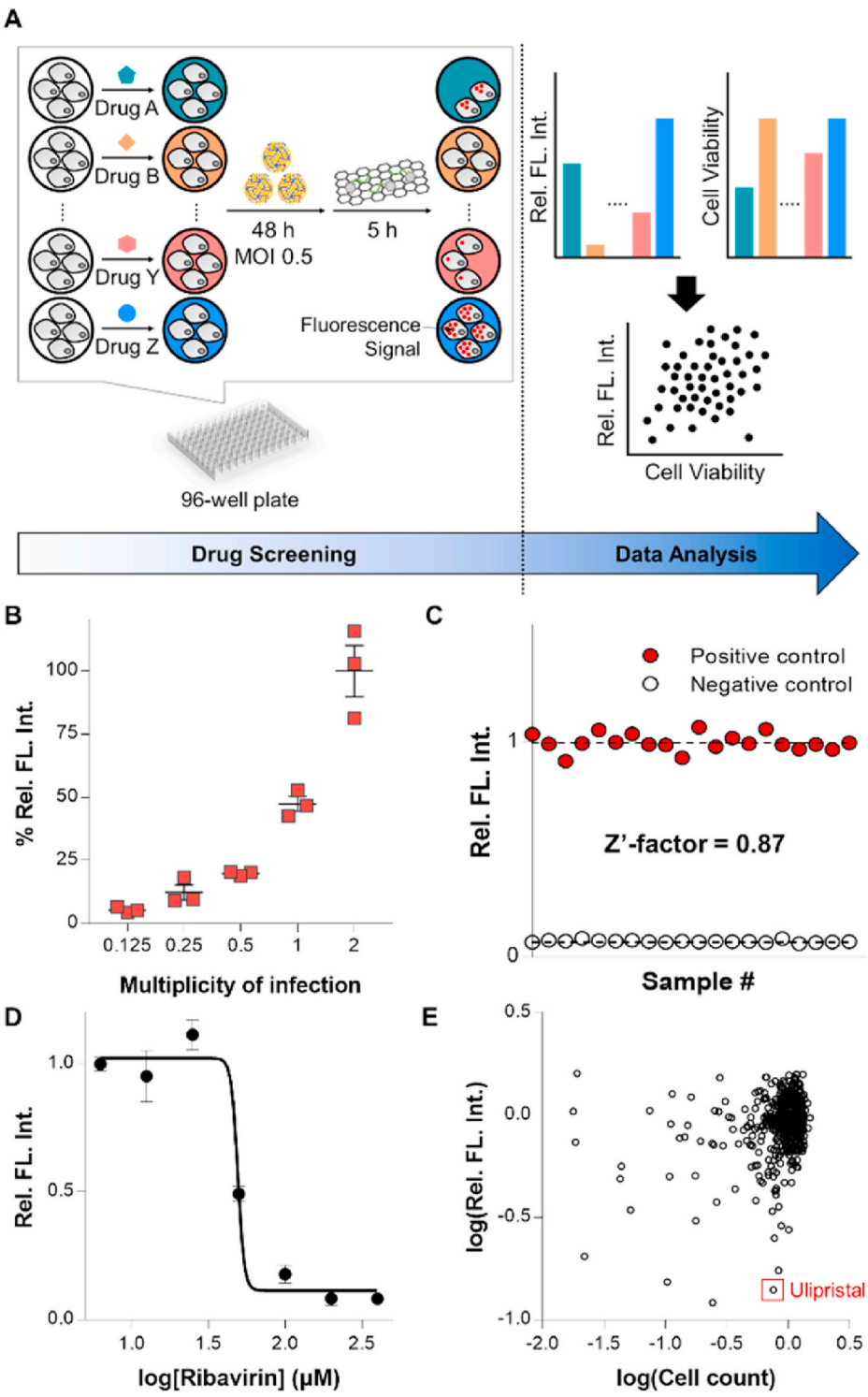

Fig. 3. The application of the GOViRA platform to high-throughput DENV inhibitor screening. (A) Schematic illustration of the GOViRA system-based high-throughput screening timeline. (B) Relative quantification of the fluorescence signal with the increasing MOI. Values represent mean ± SEM (n = 3). (C) The Z′-factor was calculated for the high-throughput screening from 20 replicates of each control. (D) DENV infection assay against ribavirin with the GOViRA system. DENV-infected Vero E6 cells were treated with ribavirin concentrations ranging from 6.25 μM to 400 μM. After 48 h, the PNA-DRGON complex was treated and DENV activity was determined. An estimated EC_{50} value against DENV serotype 2 for ribavirin was 49.2 ± 0.2 μM. Values represent mean ± SEM (n = 3). (E) A screen for anti-DENV agents was conducted. Cell viability and corresponding fluorescence intensity value for each drug are plotted.

anti-DENV activity. Vero E6 cell monolayers were treated with 10 μM of each drug in the library or with the vehicle (DMSO) for an hour before infection. Then, DENV and the PNA-DRGON complex were sequentially introduced (Fig. 3A). Based on the screening results that considered both antiviral activity and cell viability (Fig. 3E), we chose ulipristal as a potent antiviral candidate because it showed fluorescence signal decrease by <25% and minimal effects on cell viability (Fig. S7A).

3.5. *Ulipristal inhibits DENV infection in vitro*

Standard assays were done to check the antiviral effect and cytotoxicity of ulipristal *in vitro*. The activity of ulipristal against DENV was evaluated by both FFA and qRT-PCR. For the FFA, Vero E6 cells were infected with DENV in the presence of various concentrations of ulipristal. The anti-DENV activity was assessed by immunostaining with antibodies specific to the DENV E protein. As the number of foci decreased in a dose-dependent manner, FFA demonstrated that the compound does have an antiviral effect against DENV in the Vero E6

cells (Fig. S7C), and the half-effective concentration (EC_{50}) was 8.3 ± 0.1 μM (Fig. S7B). The relative expression level of viral RNA confirmed that ulipristal was active against DENV and correlated with the FFA (Fig. S7D). The cytotoxicity of the compound in the Vero E6 cells was determined by the CCK-8 assay. Ulipristal showed no impact on cell viability in the Vero E6 cells (Fig. S7D).

We further validated the antiviral activity of ulipristal using Huh7 (liver carcinoma cell line) and A549 (lung carcinoma cell line) cell lines as hosts for the DENV infection. Both cell monolayers were analyzed with qRT-PCR to observe the relative DENV RNA level. The ulipristal treatment inhibited the DENV infection in both cell lines dose-dependently (Fig. 4A and B). Moreover, the fluorescence signal of the viral E protein from immunostaining also was reduced by the ulipristal treatment (Fig. 4C). These results indicate that ulipristal effectively inhibits DENV infection *in vitro*.

3.6. Anti-DENV effect of ulipristal in murine DENV model

To confirm the antiviral activity of ulipristal in an *in vivo* DENV infection, this compound was evaluated in a murine DENV infection model. The DENV strain we used (KBPV-VR-29) has been reported as a mouse-adapted virus strain (Park et al., 2020). For our study, AG129 mice, deficient in the interferon (IFN)-α/β and –γ receptors, were infected with the DENV by intraperitoneal injection at an exposure dose of $1x10^7$ FFU which shows lethality approximately within ~10 days. One hour after the infection, the animals were treated with ulipristal or vehicle over 14 days, and survival was monitored during that period. Ulipristal was given at a dose of 15 mg/kg every day through intraperitoneal injection. The dose was determined based on the reported rodent toxicity study (Pohl et al., 2013) and our results from the *in vitro* drug validation. We attempted to select a dose that would prevent toxicity but could achieve enough plasma concentration to observe an antiviral effect.

To examine whether ulipristal treatment can relieve the symptoms in the murine DENV model, the individual mice were weighed and visually monitored for morbidity daily. Compared to the ulipristal-treated group, the control group exhibited a huge weight loss (Fig. 5A) and disease symptoms including ruffled fur, hunched posture, and decreased mobility (Shresta et al., 2006). Ulipristal treatment in the infected mice also resulted in a statistically significant survival benefit ($P = 0.0007$) shown in the survival plot (Fig. 5B). Next, we verified the systemic and local antiviral effect of ulipristal. On day 3 p.i., the ulipristal-treated group showed a significantly reduced viremia in the blood compared to that of the control group (Fig. 5C). To assess the local therapeutic effect, the viral RNA expression level in five representative organs (spleen, lung, liver, small intestine, and large intestine) and the tissue morphology were investigated. The viral RNA load in each organ of the ulipristal-administered mice was significantly decreased consistent with the viremia in the blood, although the differences between the viral RNA loads in the small intestine of the vehicle and ulipristal-treated groups were not statistically significant (Fig. 5D).

To further determine the histological differences, representative tissue samples from each group were examined (Shresta et al., 2006). Hematoxylin and eosin (H&E)-stained sections of the spleen and liver from each group were analyzed (Fig. 5E). As shown in the uninfected control group, a normal spleen shows a distinguishable white-pulp and red-pulp structure, which is severely ruptured after the virus infection (DENV infected, vehicle-treated group). It was observed that such a boundary loss was decreased in the ulipristal-treated group, indicating that the administration of ulipristal may relieve the virus infection-associated spleen damage. Moreover, several notable changes were also observed in the liver tissues as well. Pathological features of DENV infection include nuclear pleomorphism of hepatocytes, dilatation of sinusoids, and focal necrosis (labeled with black arrows). Compared to the control group, a significant reduction of such symptoms was observed in the ulipristal-treated group. Taken together, the overall data indicate that ulipristal may contribute to reducing the symptoms of DENV infection, resulting in a significant survival benefit *in vivo*.

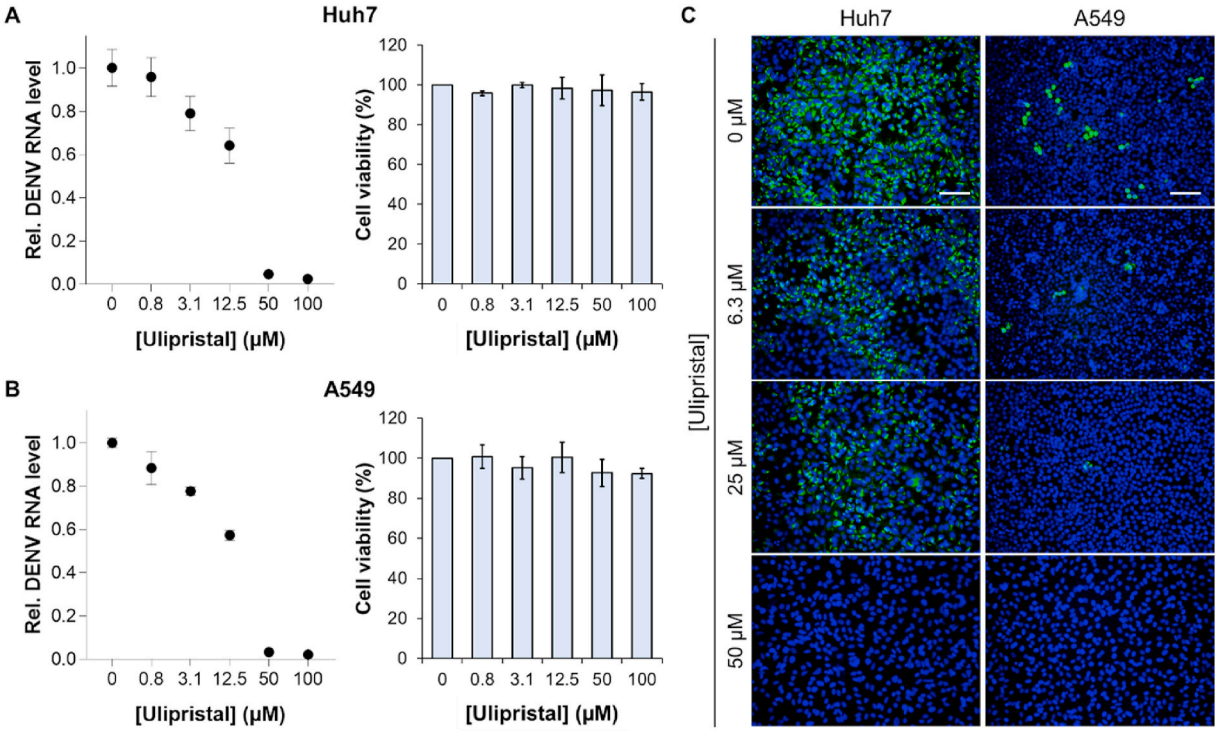

Fig. 4. Validation of ulipristal in Huh7 and A549 cells. qRT-PCR analysis of viral RNA in the DENV-infected Huh7 (A), and A549 (B) cells with dose-dependently treated ulipristal. Values represent mean ± SEM (n = 3). (C) Immunofluorescence images showing DENV E antigen (Green) and nuclei (Blue) for the dose-dependent antiviral effect of ulipristal in Huh7 and A549 cells.

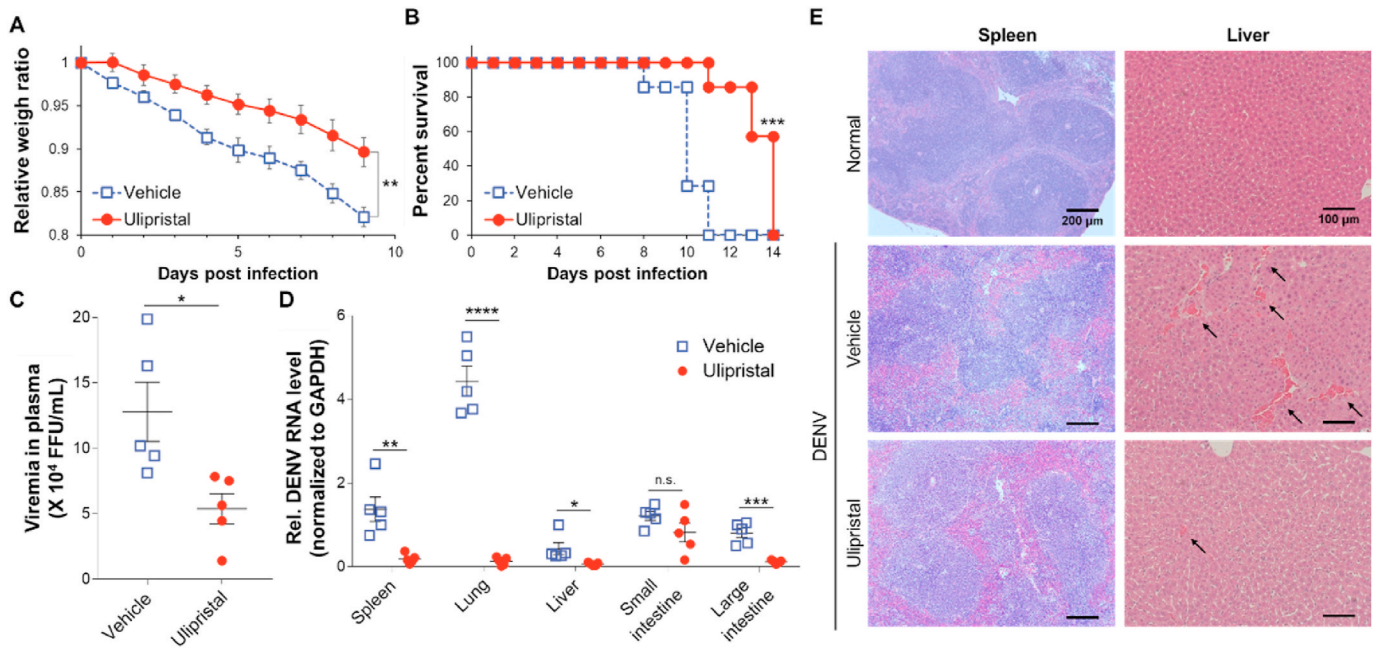

Fig. 5. ***In vivo*** **antiviral therapeutic investigation on the mouse model of DENV infection.** 15 mg/kg of ulipristal was treated once a day to DENV-infected AG129 mice. The infected mice were monitored for Relative weight changes (A), and survival plot (B). Values represent mean ± SEM (n = 7). Statistical significance was determined by Student's *t*-test (**$P \leq 0.01$; A) and log-rank test ($P = 0.0007$; B). The viremia from plasma (C), and viral RNA loads in organs (D) of DENV infected AG129 mice at 3 days p.i. Values represent mean ± SEM (n = 5). Statistical significance was determined by Student's *t*-test (n.s.: not significant, *$P \leq 0.05$, **$P \leq 0.01$, ***$P \leq 0.001$ and ****$P \leq 0.0001$; C-D). (E) H&E section micrograph images of spleen and liver from AG129 mice.

3.7. Mode of action of ulipristal is mediated by inhibiting viral entry

A time-of-addition experiment was performed to determine which time point of the viral infection stage is affected by the administration of ulipristal. Because ulipristal is widely known as an SPRM compound (Donnez et al., 2015; Richardson and Maltz 2012), we chose a cell line without PR expression to exclude the influence of PR signaling on the time-of-addition experiment. PR expression was observed in three groups of A549 cells: no treatment (NT), vehicle treatment, and ulipristal treatment group. After 24 h of incubation, the RNA expression level of each group was analyzed. There was no PR expression in the NT group (Fig. S8). Additionally, the vehicle or ulipristal treatment did not influence the levels of PR expression in the A549 cells. Therefore, we examined the mode of action of ulipristal using the A549 cell line.

A549 cells were treated with ulipristal in three different conditions: treatment before the infection (pre-treatment), treatment along with the infection (co-treatment), and treatment after the infection (post-treatment) (Fig. S9A). The antiviral effect by the administration of the drug was observed in the pre-treatment and co-treatment groups. However, a less inhibitory effect was observed when ulipristal was added after the virus inoculation. Furthermore, the degree of inhibitory effect was decreased as the ulipristal administration was delayed (Fig. S9B). Taken together, the inhibitory kinetics of ulipristal suggest that ulipristal inhibits viral infection at the entry stage of the DENV life cycle and acts as an endocytic inhibitor.

4. Discussion

Although assays for analyzing pathogens have been developed in recent years (Ganganboina et al. 2020a, 2020b), robust imaging systems that enable quantitative analysis of intracellular viral genomes in live cells remain challenging. We demonstrated that the newly developed sensitive biosensor, GOViRA, using PNA and DRGON can be used for quantitative and qualitative analysis of the intracellular DENV genome. The GOViRA system enables facile distinction between infected and non-infected cells and easily distinguishes DENV infection from other flaviviruses.

The treatment with compounds that interfere with the DENV life cycle causes a low level of intracellular DENV genome. Since it leads to a quantifiable reduction in fluorescence signal, the GOViRA system can be efficiently used for anti-DENV drug screening. We performed high-throughput screening with FDA-approved drugs and successfully identified a new drug candidate for DENV named ulipristal. The inhibitory kinetics study revealed that ulipristal inhibits viral entry into the host cell. Based on several reports depicting the successful clinical usage of viral entry inhibitors (Kilby et al., 1998; Starr-Spires and Collman 2002), it could also be suggested that ulipristal has high potential as a promising antiviral candidate for clinical use. Because the way that ulipristal mediates entry inhibition and the type of interaction that is formed with a virus or host were not fully elucidated, the precise mode of action needs to be characterized.

In the murine DENV model, it has been reported that the viremia is very low on day 1 p.i., which gradually increases and reaches its peak level on day 3 (Schul et al., 2007). Based on the viremia profile, the drug may function as an entry inhibitor by effectively blocking the initial process of infection. It is also suggested that serial treatment of ulipristal may prevent reinfection of newly produced DENV and relieve symptoms.

Ulipristal is an FDA-approved drug that has oral bioavailability and high tolerability (Bouchard and Chabbert-Buffet 2017; Del Forno et al., 2020). This makes ulipristal a promising therapeutic candidate for DENV infection. It has recently been reported by the European Medicines Agency (EMA) that ulipristal may cause drug-induced liver injury (DILI) (Meunier et al., 2020). However, the hepatic safety of ulipristal was reported by a clinical development with over 1800 patients in 2018 (Donnez et al., 2018) and the mechanism of the DILI remains unsatisfactorily explained (Meunier et al., 2020). Therefore, not only further investigations on the mechanism of the DILI but also the risk-benefit assessment of ulipristal should be considered for clinical uses.

The development of novel antiviral treatments against numerous viral diseases is in high global demand. However, the difficulty of conventional antiviral drug development includes not only the expensive,

laborious, and time-consuming process but also the uncertainty of success. The drug repurposing strategy with high-throughput screening could provide several advantages to overcome such issues. It has been one of the biggest obstacles of this approach that the simulated condition for the *in vitro* screening system could not perfectly mimic the complex and dynamic responses of the living organism in the presence of the drug. To address this challenge, our live cell-based GOViRA system can effectively identify the efficacy when the target viral disease is exposed to the compound within the context of a live cell which is a more advanced feature compared to the conventional assay systems.

5. Conclusions

In summary, this study proposes that the GOViRA platform can be helpful to study the DENV life cycle and to develop antiviral drugs. We developed a biosensor using PNA and DRGON that can quantitatively analyze the intracellular DENV genome level in live cells. In addition, anti-DENV drug repurposing through high-throughput screening was facilitated by the GOViRA platform. Through this process, ulipristal was identified as a new entry inhibitor against DENV infection having an anti-DENV activity in cells and a murine model. The repurposing of ulipristal in DENV treatment may provide great potential in clinical use. To do so, further study on the precise mode of action of ulipristal and evaluation in a non-human primate DENV infection model are necessary. The successful identification of a novel anti-DENV agent suggests that this approach can facilitate repurposing antiviral therapeutics for other various viral infections. We anticipate that the GOViRA system can accelerate the discovery of effective antiviral drug candidates at the initial stage of the drug discovery process.

Author contributions

H.S. and D.-H.M. conceived the project; H.S., S.-J.P., J.K., and J.-S.L. performed experiments; H.S. and D.-H.M. analyzed data; H.S. and D.-H. M. wrote the manuscript; D.-H.M. supervised the project.

Declaration of competing interest

The authors declare the following financial interests/personal relationships which may be considered as potential competing interests: D.-H. Min is named on patents that describe the use of nucleic acids and carbon nanomaterials as biosensors to detect nucleic acids. The remaining authors have no competing interest to declare.

Acknowledgements

This work was supported by the Basic Science Research Program (2016R1E1A1A01941202 and 2016R1A4A1010796) through the National Research Foundation of Korea (NRF), and Lemonex Inc. (LEMONEX-SN201709-3-12 and LEMONEX-SN201901-3-30).

Appendix A. Supplementary data

Supplementary data to this article can be found online at https://doi.org/10.1016/j.bios.2021.113208.

References

Barrows, N.J., Campos, R.K., Powell, S.T., Prasanth, K.R., Schott-Lerner, G., Soto-Acosta, R., Galarza-Munoz, G., McGrath, E.L., Urrabaz-Garza, R., Gao, J., Wu, P., Menon, R., Saade, G., Fernandez-Salas, I., Rossi, S.L., Vasilakis, N., Routh, A., Bradrick, S.S., Garcia-Blanco, M.A., 2016. Cell Host Microbe 20 (2), 259–270.
Boldescu, V., Behnam, M.A., Vasilakis, N., Klein, C.D., 2017. Nat. Rev. Drug Discov. 16 (8), 565–586.
Bouchard, P., Chabbert-Buffet, N., 2017. Best Pract Res Cl Ob 40, 105–110.
Chien, C.T., Li, S.S., Lai, W.J., Yeh, Y.C., Chen, H.A., Chen, I.S., Chen, L.C., Chen, K.H., Nemoto, T., Isoda, S., Chen, M., Fujita, T., Eda, G., Yamaguchi, H., Chhowalla, M., Chen, C.W., 2012. Angew Chem. Int. Ed. Engl. 51 (27), 6662–6666.
Crance, J.M., Scaramozzino, N., Jouan, A., Garin, D., 2003. Antivir. Res. 58 (1), 73–79.
Del Forno, S., Degli Esposti, E., Salucci, P., Leonardi, D., Iodice, R., Arena, A., Raimondo, D., Paradisi, R., Seracchioli, R., 2020. Gynecol. Endocrinol. 36 (5), 445–447.
Donnez, J., Arriagada, P., Marciniak, M., Larrey, D., 2018. Expet. Opin. Drug Saf. 17 (12), 1225–1232.
Donnez, J., Hudecek, R., Donnez, O., Matule, D., Arhendt, H.J., Zatik, J., Kasilovskiene, Z., Dumitrascu, M.C., Fernandez, H., Barlow, D.H., Bouchard, P., Fauser, B.C., Bestel, E., Terrill, P., Osterloh, I., Loumaye, E., 2015. Fertil. Steril. 103 (2), 519–527.
Ganganboina, A.B., Chowdhury, A.D., Khoris, I.M., Doong, R.A., Li, T.C., Hara, T., Abe, F., Suzuki, T., Park, E.Y., 2020a. Biosens. Bioelectron. 170, 112680.
Ganganboina, A.B., Khoris, I.M., Chowdhury, A.D., Li, T.-C., Park, E.Y., 2020b. ACS Appl. Mater. Interfaces 12 (45), 50212–50221.
Garcia, S., Crance, J.M., Billecocq, A., Peinnequin, A., Jouan, A., Bouloy, M., Garin, D., 2001. J. Clin. Microbiol. 39 (12), 4456–4461.
Goldoni, R., Farronato, M., Connelly, S.T., Tartaglia, G.M., Yeo, W.H., 2021. Biosens. Bioelectron. 171, 112723.
Herzog, P., Drosten, C., Muller, M.A., 2008. Virol. J. 5, 138.
Hu, Y.C., Bentley, W.E., 2000. Chem. Eng. Sci. 55 (19), 3991–4008.
Hwa, K.Y., Sharma, T.S.K., Ganguly, A., 2020. Inorg Chem Front 7 (10), 1981–1994.
Kilby, J.M., Hopkins, S., Venetta, T.M., DiMassimo, B., Cloud, G.A., Lee, J.Y., Alldredge, L., Hunter, E., Lambert, D., Bolognesi, D., Matthews, T., Johnson, M.R., Nowak, M.A., Shaw, G.M., Saag, M.S., 1998. Nat. Med. 4 (11), 1302–1307.
Kuno, G., Chang, G.J., Tsuchiya, K.R., Karabatsos, N., Cropp, C.B., 1998. J. Virol. 72 (1), 73–83.
Lee, J.S., Kim, S., Na, H.K., Min, D.H., 2016. Adv Healthc Mater 5 (18), 2386–2395.
Loh, K.P., Bao, Q., Eda, G., Chhowalla, M., 2010. Nat. Chem. 2 (12), 1015–1024.
Martina, B.E., Koraka, P., Osterhaus, A.D., 2009. Clin. Microbiol. Rev. 22 (4), 564–581.
Meunier, L., Meszaros, M., Pageaux, G.P., Delay, J.M., Herrero, A., Pinzani, V., Dominique, H.B., 2020. Clin Res Hepatol Gastroenterol 44 (3), e45–e49.
Mukherjee, S., Sirohi, D., Dowd, K.A., Chen, Z.G., Diamond, M.S., Kuhn, R.J., Pierson, T. C., 2016. Virology 497, 33–40.
Park, J.S., Na, H.K., Min, D.H., Kim, D.E., 2013. Analyst 138 (6), 1745–1749.
Park, S.J., Kim, J., Kang, S., Cha, H.J., Shin, H., Park, J., Jang, Y.S., Woo, J.S., Won, C., Min, D.H., 2020. Sci Adv 6 (22), eaaz8201.
Pohl, O., Harvey, P.W., McKeag, S., Boley, S.E., Gotteland, J.P., 2013. Curr. Drug Saf. 8 (2), 77–97.
Pushpakom, S., Iorio, F., Eyers, P.A., Escott, K.J., Hopper, S., Wells, A., Doig, A., Guilliams, T., Latimer, J., McNamee, C., Norris, A., Sanseau, P., Cavalla, D., Pirmohamed, M., 2019. Nat. Rev. Drug Discov. 18 (1), 41–58.
Qing, M., Liu, W., Yuan, Z., Gu, F., Shi, P.Y., 2010. Antivir. Res. 86 (2), 163–171.
Richardson, A.R., Maltz, F.N., 2012. Clin. Therapeut. 34 (1), 24–36.
Ryoo, S.R., Lee, J., Yeo, J., Na, H.K., Kim, Y.K., Jang, H., Lee, J.H., Han, S.W., Lee, Y., Kim, V.N., Min, D.H., 2013. ACS Nano 7 (7), 5882–5891.
Schul, W., Liu, W., Xu, H.Y., Flamand, M., Vasudevan, S.G., 2007. J. Infect. Dis. 195 (5), 665–674.
Sharma, T.S.K., Hwa, K.-Y., 2020. J Hazard Mater. https://doi.org/10.1016/j.jhazmat.2020.124659.
Shresta, S., Sharar, K.L., Prigozhin, D.M., Beatty, P.R., Harris, E., 2006. J. Virol. 80 (20), 10208–10217.
Starr-Spires, L.D., Collman, R.G., 2002. Clin. Lab. Med. 22 (3), 681–701.
Stender, H., Fiandaca, M., Hyldig-Nielsen, J.J., Coull, J., 2002. J. Microbiol. Methods 48 (1), 1–17.
Wilder-Smith, A., Ooi, E.E., Horstick, O., Wills, B., 2019. Lancet 393 (10169), 350–363.
Xu, Z., Lei, X., Tu, Y., Tan, Z.J., Song, B., Fang, H., 2017. Chemistry 23 (53), 13100–13104.
Ye, C., Wang, D., Liu, H., Ma, H., Dong, Y., Yao, M., Wang, Y., Zhang, H., Zhang, L., Cheng, L., Xu, Z., Lei, Y., Zhang, F., Ye, W., 2019. Front. Pharmacol. 10, 1203.
Zhang, B., Wei, P., Zhou, Z.X., Wei, T.T., 2016. Adv. Drug Deliv. Rev. 105, 145–162.
Zhang, J.H., Chung, T.D.Y., Oldenburg, K.R., 1999. J. Biomol. Screen 4 (2), 67–73.
Zou, G., Xu, H.Y., Qing, M., Wang, Q.Y., Shi, P.Y., 2011. Antivir. Res. 91 (1), 11–19.